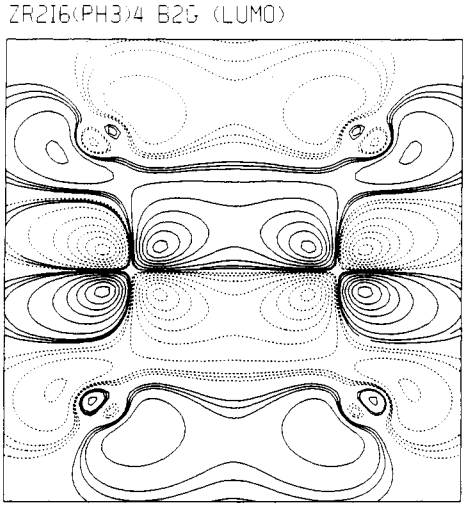

Figure 4. Contour plot of the B_{2g} LUMO of $Zr_2I_6(PH_3)_4$, in the *xz* plane.

calculation resulted in a molecular orbital diagram with 41 doubly occupied valence orbitals. The HOMO is formed, primarily, from a combination of zirconium d_{z^2} and $d_{x^2-y^2}$ orbitals (the combined metal character is 92.6%). The bridging iodide atoms interact only weakly along the Zr-I_b vectors, through a linear combination of their p_y and p_z orbitals (combined I_b character in the HOMO is 2.8%). We and others believe that the long metal-metal interaction in these complexes is best described as being, primarily, through-space.[22] A contour plot of the HOMO of $Zr_2I_6(PH_3)_4$, in the *xz* plane, is given in Figure 3. Clearly, this orbital provides a significant M-M σ bond. The LUMO is composed of zirconium d_{xz} π-type orbitals, which lie in a plane perpendicular to the $Zr_2(I_b)_2$ plane. A contour plot of the LUMO, in the *xz* plane, is given in Figure 4.

Concluding Remarks

The $M_2I_6(PR_3)_4$ complexes are structurally similar to previously reported group IV metal chloride-bridged bioctahedral complexes, the main distinction being the considerably longer metal-metal distance. Structural and theoretical data concur in suggesting that these diamagnetic complexes are correctly formulated with long but real metal-metal single bonds. We are currently attempting to synthesize and structurally characterize edge-sharing dimers of zirconium and hafnium with other atoms in the bridging position, for comparative purposes.

Acknowledgment. We thank Judith L. Eglin for carrying out the ^{31}P NMR spectroscopy and the Robert A. Welch Foundation for support under Grant A 494.

Supplementary Material Available: Full listings of bond lengths and angles, thermal displacements, and valence molecular orbitals, their energies, and percent characters for $Zr_2I_6(PH_3)_6$ (39 pages); tables of observed and calculated structure factors for **1-3** (35 pages). Ordering information is given on any current masthead page.

Contribution from the Department of Chemistry and Laboratory for Molecular Structure and Bonding, Texas A&M University, College Station, Texas 77843

Preparation and Molecular and Electronic Structures of a New Diamagnetic Diruthenium(II) Complex, $Ru_2[(p\text{-tol})NC(H)N(p\text{-tol})]_4$

F. Albert Cotton* and Tong Ren

Received March 15, 1991

The title complex, $Ru_2(DFM)_4$ (DFM^- = (*p*-tol)NCHN(*p*-tol)$^-$), has been synthesized and characterized by X-ray crystallography as well as several spectroscopic methods. The dark red complex crystallizes as $Ru_2(DFM)_4 \cdot C_6H_6$ in space group *Pbnb* with a = 17.086 (4) Å, b = 23.952 (11) Å, c = 15.521 (4) Å, V = 6352 (4) Å^3, and Z = 4. The complex has been shown to be diamagnetic on the basis of ^1H NMR spectroscopy and has a very long Ru-Ru distance (2.474 (1) Å). These features are indicative of a $(\sigma)^2(\pi)^4(\delta)^2(\pi^*)^4$ ground-state configuration. A fairly large $\delta^*-\pi^*$ gap (1.18 eV) was derived from an SCF-Xα calculation performed on the model $Ru_2(HNCHNH)_4$, thus confirming the configuration mentioned above. The observed electronic absorption spectrum was assigned with the aid of the MO calculation.

Introduction

Recent studies of diruthenium chemistry have shown that the diruthenium(II) complexes, that is, those with a Ru_2^{4+} core, provide a valuable test ground for the development of metal-metal bonding theory.[1-9] As discussed earlier for various $Ru_2(LL)_4$ species,[2,5,8] for a d^6-d^6 system in an effective D_{4h} symmetry there are three possible ground-state configurations beyond the $(\sigma)^2(\pi)^4(\delta)^2$ shells, namely, $(\pi^*)^4$, $(\pi^*)^3(\delta^*)$, and $(\pi^*)^2(\delta^*)^2$. The category to which a particular complex belongs is determined by the $\delta^*-\pi^*$ separation, which is in turn determined by the π basicity of the bridging ligand LL^-. Among all known diruthenium(II) complexes, triazeno complexes distinguish themselves in being diamagnetic at room temperature and having a very long Ru-Ru bond length.[4-6] A large $\delta^*-\pi^*$ gap of 0.98 eV was found through a model Xα calculation,[7] which, in conjunction with the structural and NMR evidence, has convincingly shown that $(\pi^*)^4$ is the ground-state configuration. Here we report the synthesis and various characterizations of another diamagnetic diruthenium(II) complex, $Ru_2[(p\text{-tol})NCHN(p\text{-tolyl})]_4$.

Experimental Section

The synthesis and the spectroscopic characterizations were carried out in argon atmosphere by using standard Schlenkware and some other air-tight containers. $Ru_2(OAc)_4$ was prepared by refluxing the reduced "blue solution" of ruthenium trichloride with LiOAc in MeOH under argon;[1] di-*p*-tolylformamidine (HDFM) was obtained by the direct condensation between triethyl orthoformate and *p*-toluidine.[10] All the solvents used were freshly distilled over suitable drying reagents under N_2.

Preparation of $Ru_2(DFM)_4$. A 1.01-g amount of HDFM (4.5 mmol) was dissolved in 15 mL of THF, and the solution was then neutralized

* To whom correspondence should be addressed.

(1) Lindsay, A. J.; Wilkinson, G.; Motevalli, M.; Hursthouse, M. B. *J. Chem. Soc., Dalton Trans.* **1985**, 2321.
(2) Cotton, F. A.; Miskowski, V. M.; Zhong, B. *J. Am. Chem. Soc.* **1989**, *111*, 6177.
(3) Maldivi, P.; Giroud-Godquin, A.; Marchon, J.; Guillon, D.; Skoulios, A. *Chem. Phys. Lett.* **1989**, *157*, 552.
(4) Lindsay, A. J.; Wilkinson, G.; Motevalli, M.; Hursthouse, M. B. *J. Chem. Soc., Dalton Trans.* **1987**, 2723.
(5) Cotton, F. A.; Matusz, M. *J. Am. Chem. Soc.* **1988**, *110*, 5761.
(6) Cotton, F. A.; Falvello, L. R.; Ren, T.; Vidyasagar, K. Manuscript in preparation.
(7) Cotton, F. A.; Feng, X. *Inorg. Chem.* **1989**, *28*, 1180.
(8) Cotton, F. A.; Ren, T.; Eglin, J. L. *J. Am. Chem. Soc.* **1990**, *112*, 3439.
(9) Cotton, F. A.; Ren, T.; Eglin, J. L. *Inorg. Chem.* **1991**, *30*, 2552.
(10) Bradley, W.; Wright, I. *J. Chem. Soc.* **1956**, 640.

0020-1669/91/1330-3675$02.50/0

Table I. Crystallographic Parameters for $Ru_2(DFM)_4 \cdot 2C_6H_6$

chem formula	$Ru_2N_8C_{72}H_{72}$
fw	1251.6
space group	*Pbnb* (No. 56)
systematic abs	*hk*0 and 0*kl*, $k = 2n$; *h*0*l*, $h + l = 2n$
a, Å	17.086 (4)
b, Å	23.952 (11)
c, Å	15.521 (4)
V, Å^3	6352 (4)
Z	4
d_{calc}, g cm^{-3}	1.309
μ, cm^{-1}	5.1
λ(Mo Kα), Å	0.710 73
data collcn instrument	Enraf-Nonius CAD-4
T, °C	−40 ± 1
transm coeff: max; min	1.00; 0.82
R^a	0.060
$R_w{}^b$	0.065

$^a R = \sum||F_o| - |F_c||/\sum|F_o|$. $^b R_w = [\sum w(|F_o| - |F_c|)^2/\sum w|F_o|^2]^{1/2}$; $w = 1\sigma^2(|F_o|)$.

by the addition of 2.9 mL of 1.6 M *n*-BuLi (in hexane) at −78 °C. After warming to room temperature the yellow lithium salt was transferred via cannula to a suspension of 0.44 g of $Ru_2(OAc)_4$ (1.0 mmol) in 20 mL of THF. The mixture was stirred at room temperature and gradually became deep red over a period of 30 min. The reaction was stopped after 8 h, and the reaction mixture was dried under vacuum. The solid residue was washed with methanol until the washings became pale red and then further washed with 2 × 10 mL of hexane. The bright red solid was dried and finally recrystallized from hot toluene to give 0.51 g (47%) of microcrystalline product. The complex is very air sensitive. On exposure to air in solution it turned to deep purple immediately, and as a wet solid, it did so over several hours. However the vacuum-dried sample is stable in dry air for several days. The sample also decomposed in $CDCl_3$ even under an inert atmosphere. Crystals suitable for X-ray analysis were grown by slow diffusion of hexane into a benzene solution of the product. The pure complex can interact with various Ag^+ salts to give a purple product, which has not been successfully crystallized.

^{1}H NMR (C_6D_6 (ppm)): 7.06 (d, aromatic protons), 6.61 (d, aromatic protons), and 2.30 (s, CH_3). UV–vis–near-IR (benzene)[λ, nm (ε, M^{-1} cm^{-1})]: 905 (3002), ca. 540 (sh, ca. 4900), 492 (8780), 434 (6250), 396 (7150), ca. 305 nm (sh, ca. 42 500). IR (cm^{-1}): 1608 (m), 1505 (s), 1219 (s), 1177 (m), 1113 (w), 931 (w), 815 (s), 719 (w), 519 (m), 419 (m).

Physical Measurements. The UV–vis-near-IR spectrum (950–250 nm) was measured on a Cary 17D spectrometer at ambient temperature with a quartz cell. The ^{1}H NMR spectrum was recorded on a Varian-200 spectrometer. The IR spectrum was recorded with an IBM IR/44 FT-IR instrument having a range 4000–400 cm^{-1}. The spectra of solid samples were taken as Nujol mulls between CsI plates. Cyclic voltammograms were recorded on a BAS 100 electrochemical analyzer in 0.2 M $(n\text{-Bu})_4NBF_4$ solution (CH_2Cl_2) with a Pt working electrode and a Ag/AgCl reference electrode. Ferrocene was oxidized at 450 mV under the experimental conditions.

X-ray Crystallography. A dark red platelike crystal was mounted on the top of a quartz fiber with epoxy resin and kept at −40 °C during the data collection. An orthorhombic cell was derived from the initial indexing, and further confirmed by axial oscillation photographs. The space group was uniquely determined as *Pbnb* (nonstandard setting of *Pccn*, No. 56) from the systematic absences. Diffraction data were collected on an Enraf-Nonius CAD-4 diffractometer using monochromated Mo Kα radiation. The description of the equipment and the detailed discussion of the normal crystallographic procedures we followed are presented elsewhere.[11,12] The data set was corrected for Lorentz and polarization effects, while no decay correction was appliedd since there was no observable decay during the data collection. An empirical absorption correction based on the ψ-scan method was also applied to the data.[13] The Patterson method was used to locate the ruthenium atoms. The rest of the non-hydrogen atoms in the molecule were found by routine methods referred to above. Two ruthenium atoms reside on the crystallographic 2-fold axis. After all these atoms were refined with anisotropic thermal parameters to a low residual, a benzene molecule was found at a general position from the difference Fourier map. This solvent molecule did not refine well during the subsequent refinement steps. It was later refined as a rigid-body hexagon with SHELX-76 to a low residual. The final figures of merit and the fractional coordinates of all atoms are listed in Tables I and II, respectively.

Table II. Positional Parameters and Their Estimated Standard Deviations for $Ru_2(DFM)_4 \cdot 2C_6H_6$

atom	*x*	*y*	*z*	B,^{a} Å^2
Ru(1)	0.250	0.11216 (3)	0.250	1.96 (2)
Ru(2)	0.250	0.00882 (3)	0.250	1.86 (2)
N(1)	0.2877 (4)	0.1085 (3)	0.1251 (5)	2.2 (2)
N(2)	0.1365 (4)	0.1083 (3)	0.2083 (5)	2.2 (2)
N(3)	0.3061 (4)	0.0125 (3)	0.1340 (5)	2.3 (2)
N(4)	0.3544 (4)	0.0126 (3)	0.3107 (4)	2.3 (2)
C(1)	0.3107 (5)	0.0600 (4)	0.0919 (6)	2.6 (2)
C(2)	0.1061 (5)	0.0606 (4)	0.1824 (5)	2.5 (2)
C(3)	0.2818 (5)	0.1545 (4)	0.0665 (6)	2.4 (2)
C(4)	0.3102 (6)	0.2065 (4)	0.0911 (7)	3.2 (2)
C(5)	0.3046 (6)	0.2520 (5)	0.0350 (7)	3.6 (2)
C(6)	0.2464 (7)	0.1481 (4)	−0.0114 (6)	4.0 (2)
C(7)	0.2409 (7)	0.1937 (4)	−0.0678 (7)	4.4 (3)
C(8)	0.2710 (6)	0.2464 (5)	−0.0443 (8)	4.0 (3)
C(9)	0.2678 (8)	0.2964 (5)	−0.1056 (9)	6.6 (4)
C(10)	0.0860 (5)	0.1552 (4)	0.2119 (6)	2.4 (2)
C(11)	0.1125 (5)	0.2075 (4)	0.1855 (6)	2.6 (2)
C(12)	0.0622 (6)	0.2544 (4)	0.1893 (7)	3.2 (2)
C(13)	0.0096 (5)	0.1487 (4)	0.2439 (7)	3.4 (2)
C(14)	−0.0404 (6)	0.1949 (4)	0.2462 (8)	4.1 (2)
C(15)	−0.0148 (7)	0.2482 (5)	0.2178 (7)	3.7 (2)
C(16)	−0.0700 (7)	0.2977 (5)	0.2194 (9)	5.2 (3)
C(17)	0.3465 (6)	−0.0336 (4)	0.0995 (6)	2.6 (2)
C(18)	0.3082 (6)	−0.0850 (4)	0.0870 (7)	3.5 (2)
C(19)	0.3479 (7)	−0.1306 (5)	0.0543 (7)	4.0 (3)
C(20)	0.4275 (7)	−0.0281 (5)	0.0817 (8)	4.5 (3)
C(21)	0.4663 (7)	−0.0749 (6)	0.0470 (8)	4.8 (3)
C(22)	0.4286 (8)	−0.1253 (5)	0.0311 (6)	3.9 (3)
C(23)	0.4717 (9)	−0.1747 (6)	−0.0081 (8)	6.3 (4)
C(24)	0.3880 (5)	−0.0347 (4)	0.3530 (6)	2.3 (2)
C(25)	0.4141 (6)	−0.0305 (5)	0.4380 (7)	3.7 (3)
C(26)	0.4475 (7)	−0.0770 (5)	0.4775 (8)	4.1 (3)
C(27)	0.3918 (6)	−0.0862 (4)	0.3116 (6)	3.3 (2)
C(28)	0.4245 (6)	−0.1319 (4)	0.3557 (7)	3.3 (2)
C(29)	0.4543 (6)	−0.1260 (5)	0.4376 (7)	3.5 (3)
C(30)	0.4934 (7)	−0.1763 (6)	0.4797 (9)	5.9 (4)
C(31)	0.391 (1)	0.010 (1)	0.686 (2)	15.9 (9)*
C(32)	0.405 (1)	0.026 (1)	0.771 (2)	22 (1)*
C(33)	0.379 (1)	−0.008 (1)	0.838 (2)	18 (1)*
C(34)	0.341 (1)	−0.058 (1)	0.821 (2)	28 (2)*
C(35)	0.328 (1)	−0.074 (1)	0.735 (2)	23 (1)*
C(36)	0.353 (1)	−0.040 (1)	0.668 (2)	28 (2)*

^{a} Starred B values are for atoms that were refined isotropically. B values for anisotropically refined atoms are given in the form of the equivalent isotropic displacement parameter defined as $(4/3)[a^2\beta_{11} + b^2\beta_{22} + c^2\beta_{33} + ab(\cos\gamma)\beta_{12} + ac(\cos\beta)\beta_{13} + bc(\cos\alpha)\beta_{23}]$.

Computational Procedure. A restricted SCF-Xα calculation[14] was used to study the electronic structure. Norman's overlapping atomic sphere radii[15] were taken to be 88.5% of the atomic number radii. The outer sphere was made tangent to the outer atomic spheres. The α values of the atoms were taken from Schwartz,[16] and the one for both intersphere and outer sphere was taken as the valence electron weighted average of the atomic α. The SCF iteration was considered to be converged if the potential change was less than 0.001 Ry. The model complex for $Ru_2(DFM)_4$ was chosen as $Ru_2(HNCHNH)_4$. The validity of this simplification has been justified in previous Xα studies of $Ru_2[(p\text{-tol})NNN(p\text{-tol})]_4$ and $Mo_2[(p\text{-tol})NCHN(p\text{-tol})]_4$.[7,15] The model molecule possessed D_{4h} symmetry. The bond lengths and angles of the model were obtained by averaging the crystallographic data of the real molecule

(11) Bino, A.; Cotton, F. A.; Fanwick, P. E. *Inorg. Chem.* **1979**, *18*, 3558.
(12) Cotton, F. A.; Frenz, B. A.; Deganello, G.; Shaver, A. *J. Organomet. Chem.* **1973**, *50*, 227.
(13) North, A. C. T.; Phillips, D. C.; Mathews, F. S. *Acta Crystallogr., Sect. A: Cryst. Phys., Diffr., Theor. Gen. Crystallogr.* **1968**, *24A*, 351.
(14) (a) Slater, J. C. *Quantum Theory of Molecules and Solids*; McGraw-Hill: New York, 1974. (b) Johnson, K. H. *Adv. Quantum Chem.* **1973**, *7*, 143. (c) Connolly, J. W. D. In *Semiempirical Methods of Electronic Structure Calculation. Part A: Techniques*; Segal, G. A., Ed.; Plenum Press: New York, 1977. (d) A version of the SCF-Xα program package of M. Cook (Harvard), modified by B. E. Bursten and G. G. Stanley (Texas A&M University), was used.
(15) Norman, J. G., Jr. *Mol. Phys.* **1976**, *31*, 1191.
(16) Schwartz, K. *Phys. Rev.* **1972**, *5*, 2466.

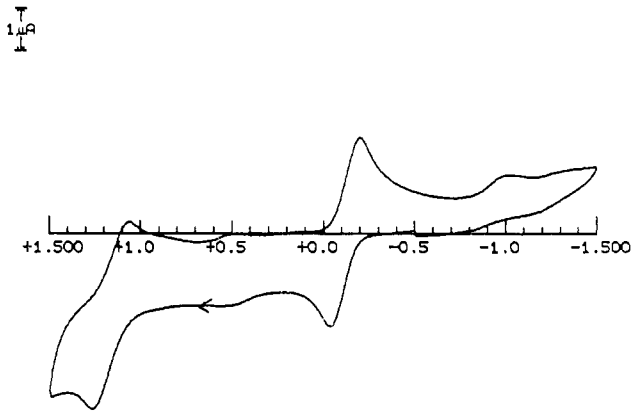

Figure 1. Cyclic voltammogram of $Ru_2(DFM)_4$ (scan speed 200 mV/s).

Table III. Selected Bond Distances (Å) and Angles (deg) for $Ru_2(DFM)_4 \cdot 2C_6H_6$[a]

Bond Distances			
Ru(1)-Ru(2)	2.475 (1)	N(1)-C(1)	1.330 (11)
Ru(1)-N(1)	2.045 (7)	N(2)-C(2)	1.318 (12)
Ru(1)-N(2)	2.046 (7)	N(3)-C(1)	1.313 (12)
Ru(2)-N(3)	2.041 (7)	N(4)-C(2)	1.337 (12)
Ru(2)-N(4)	2.019 (7)		
Bond Angles			
Ru(2)-Ru(1)-N(1)	87.5 (2)	Ru(1)-N(2)-C(2)	120.7 (6)
Ru(2)-Ru(1)-N(2)	87.4 (2)	Ru(2)-N(3)-C(1)	120.3 (6)
Ru(1)-Ru(2)-N(3)	87.5 (2)	Ru(2)-N(4)-C(2)	121.5 (6)
Ru(1)-Ru(2)-N(4)	87.4 (2)	N(1)-C(1)-N(3)	123.1 (8)
Ru(1)-N(1)-C(1)	119.8 (6)	N(2)-C(2)-N(4)	121.4 (8)

[a] Numbers in parentheses are estimated standard deviations in the least significant digits.

as follows: Ru-Ru = 2.474 Å, Ru-N = 2.034 Å, N-C = 1.312 Å, Ru-Ru-N = 87.1°, and Ru-N-C = 121.8°, and the C-H and N-H bond lengths were assumed to be 1.10 and 1.00 Å, respectively.

On the basis of the converged potential of the restricted SCF calculation, the transition-state technique[14] was applied to estimate the state-to-state energy of several transitions. The excitation energy of both singlet–singlet and singlet–triplet transitions were derived from two separate spin-unrestricted SCF iterations.[17] The convergence criterion for such a transition-state iteration was that the potential shift be less than 0.002 Ry.

Results and Discussion

The synthetic route for $Ru_2(DFM)_4$ is very similar to that used for the triazeno complex

$$Ru_2(OAc)_4 + 4LiDFM \rightarrow Ru_2(DFM)_4 + 4LiOAc\downarrow$$

This reaction proceeds more easily than the reactions for the tirazeno complex (24 h reaction time) judging from the time required. The precipitation of LiOAc from THF is probably one reason for this. This compound, for some unknown reason, is much more air sensitive than the triazeno analogue, and hence great care is necessary in handling it. The cyclic voltammogram, as presented in Figure 1, reveals that there is a reversible oxidation at 1.163 V, as well as a reversible reduction at −0.118 V. The oxidation potential is substantially higher than those observed for the triazeno complexes (ca. 0.16 V for PhN_3Ph and 0.28 V for $(p\text{-tol})N_3(p\text{-tol})$), and reversible reduction was not observed for triazeno complexes. The nature of the redox behavior is not well understood, since the oxidation potential suggests that the complex should be quite stable toward oxygen. The proton NMR spectrum showed the normal signals for the tolyl group, which shows that the complex is not paramagnetic at room temperature.

The $Ru_2(DFM)_4$ molecule, as shown in Figure 2, assumed the bidentate bridging coordination geometry that is common for $M_2(DFM)_4$. Some important bond distances and bond angles are listed in Table III. The most notable feature of this molecule

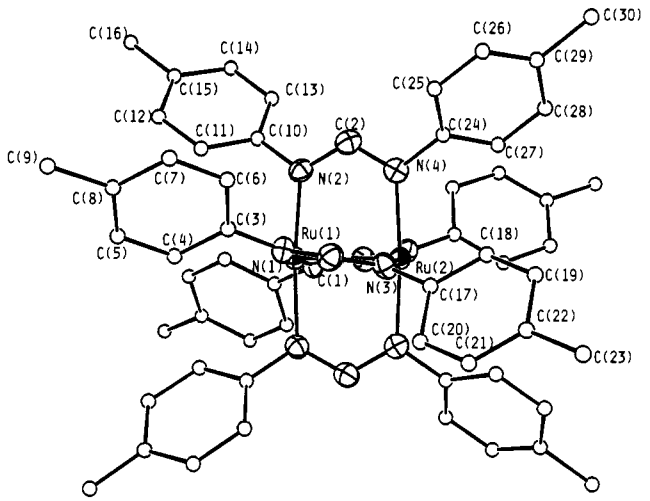

Figure 2. ORTEP drawing of $Ru_2(DFM)_4$.

is that the Ru-Ru distance, 2.474 (1) Å, is longer than the corresponding ones in $Ru_2[(p\text{-tol})N_3(p\text{-tol})]_4$[5] and $Ru_2(PhN_3Ph)_4$[6] by 0.057 and 0.075 Å, respectively. It is, in fact, the longest Ru-Ru distance among all known $Ru_2(LL)_4$ type complexes. We do not believe the lengthening of the Ru-Ru bond is due to the increased spacing between the two coordinating nitrogen atoms (i.e. the "bite") of the ligand. Although this distance (2.32 Å) is longer than that in the PhN_3Ph^- case (2.22 Å), the flexibility of DFM^- can be seen from the fact that the bite was 2.21 Å in $Mo_2(DFM)_4$ with a Mo-Mo bond length 2.085 Å[18] and 2.29 Å in $Cr_2(DFM)_4$ with a Cr-Cr distance 1.927 Å.[19] Also diformanidinato ligands have been found to coordinate in the chelating forms in various coordination compounds.[20-22] Therefore, an electronic rather than a steric perturbation from the ligand is probably the dominant factor in determining the Ru-Ru bond length.

As discussed in several earlier accounts of diruthenium(II) complexes,[2,4,5,7,8] the only rationale for both the diamagnetism and the long Ru-Ru spacing is the assignment of a $(\sigma)^2(\pi)^4(\delta)^2(\pi^*)^4$ gound-state configuration. This means that a formal double bond exists between the ruthenium atoms. It may seem anomalous that this Ru-Ru double bond is slightly longer than the Rh-Rh single bond (2.434 Å) in the analogous $Rh_2(DFM)_4$,[23] but this relationship may be understood in terms of both the weakness of the δ component and the larger covalent radius of Ru(II). A slight distortion from the ideal eclipsed configuration was also observed for the molecule, which has the torsional angles of 9.66 (0.29)° (N(1)-Ru(1)-Ru(2)-N(3)) and 9.40 (0.28)° (N(2)-Ru(1)-Ru(2)-N(4)).

The SCF-Xα method has proved to be an effective theoretical tool for the complexes containing metal-metal multiple bonds, since electron correlation has been partially included in the Slater exchange potential. We have employed the restricted Xα calculation on a model molecule, $Ru_2(HNCHNH)_4$, with strict D_{4h} symmetry. The energy levels and charge distributions of the upper valence molecular orbitals of the converged SCF iteration are listed in Table IV. The low-energy, ligand-dominated orbitals (C-H, N-H, and N-C σ bond) have little relevance to our discussion and hence have been omitted.

(17) Cotton, F. A.; Feng, X.; Matusz, M. M. *Inorg. Chem.* **1989**, *28*, 594.

(18) Ziegler, T. In *Local Density Approximation in Quantum Chemistry and Solid State Physics*; Dahl, J. P., Avery, J., Eds.; Plenum: New York, 1984.

(19) Cotton, F. A.; Ren, T. Unpublished structure determination of $Cr_2(DFM)_4$.

(20) Ibers, J. A. In *Transition Metal Hydrides*; Bau, R., Ed.; American Chemical Society: Washington, DC, 1978.

(21) De Roode, W. H.; Vrieze, K.; Koerner von Gustorf, E. A.; Ritter, A. *J. Organomet. Chem.* **1977**, *135*, 183.

(22) Cotton, F. A.; Ren, T. Unpublished synthesis and structural characterization of $W_2(\mu_2\text{-}OH)_2(DFM)_4$.

(23) Piraino, P.; Bruno, G.; Schiavo, S. L.; Laschi, F.; Zanello, P. *Inorg. Chem.* **1987**, *26*, 2205.

Table IV. Upper Valence Molecular Orbitals for $Ru_2(HNC(H)NH)_4$[a]

		% charge					Ru angular contribn, %		
level	*E*, eV	Ru	N	C	H_n	H_c	s	p	d
$5a_{2u}$	−2.109	71	26	3	0	0			99
$6a_{1g}$	−2.613	47	43	7	0	3		50	50
$4a_{2u}$	−4.837	91	8	0	1	0	6	5	90
$2b_{1u}$	−5.152	67	33	0	0	0			100
$5e_g$	−6.333	96	3	0	1	0			100
$1a_{1u}$	−6.594	0	100	0	0	0			
$2b_{2g}$	−6.780	84	3	13	0	0			100
$4e_g$	−7.193	2	98	0	0	0			
$6e_u$	−7.644	81	15	0	3	1		2	98
$5a_{1g}$	−8.279	87	9	2	0	2	19	2	79
$5e_u$	−8.858	24	52	12	2	10		25	75
$1b_{1u}$	−9.452	48	52	0	0	0			100
$1a_{2g}$	−9.936	0	65	35	0	0			
$3e_g$	−10.042	9	80	2	9	0			
$4e_u$	−10.600	3	65	30	0	2			
$4a_{1g}$	−10.924	31	38	12	5	14	14		86
$4b_{1g}$	−11.276	35	34	12	4	15			100
$1b_{2g}$	−11.610	18	60	22	0	0			100
$3a_{2u}$	−12.066	24	62	1	13	0	34	1	65
$3b_{2u}$	−12.432	33	54	0	13	0			100

[a] % charge indicates relative amount of charge in the atomic spheres, and metal angular contribution is given only when >10%.

Table V. Calculated Transition Energies (cm^{-1}) for $Ru_2(DFM)_4$

transition	type	dipole[a]	E_s[b]	E_T[b]
$5e_g \rightarrow 2b_{1u}$	$\pi^* \rightarrow \delta^*$	A, (*x*,*y*)	11740 (1.445)	7900 (0.979)
$5e_g \rightarrow 4a_{2u}$	$\pi^* \rightarrow \sigma^*$	A, (*x*,*y*)	14280 (1.771)	10400 (1.289)
$2b_{2g} \rightarrow 2b_{1u}$	$\delta \rightarrow \delta^*$	A, *z*	14490 (1.797)	11900 (1.475)
$2b_{2g} \rightarrow 4a_{2u}$	$\delta \rightarrow \sigma^*$	F		
$4e_g \rightarrow 2b_{1u}$	$\pi(N) \rightarrow \delta^*$	A, (*x*,*y*)	18320 (2.272)	17160 (2.128)
$4e_g \rightarrow 4a_{2u}$	$\pi(N) \rightarrow \sigma^*$	A, (*x*,*y*)	20700 (2.566)	20260 (2.512)

[a] A = dipole allowed; F = dipole-forbidden. [b] $E_{S(T)}$ values are the transition energies in cm^{-1} (eV in parentheses) for singlet to singlet (triplet) transitions.

The electronic structure of $Ru_2(DFM)_4$ was expected to be similar to that encountered in the triazeno complex, considering the similarity of the ligand structures and the room-temperature diamagnetism common to both, as shown by ^1H NMR spectra. The model Xα calculation did show marked resemblances in both the distribution of energy levels and the atomic charge contributions (see Table III and ref 7). The molecular orbitals with dominant metal–metal bonding or antibonding character are, in ascending energy order, $5a_{1g}$ (σ), $6e_u$ (π) $2b_{2g}$ (δ), $5e_g$ (π^*, HOMO), $2b_{1u}$ (δ^*, LUMO) and $4a_{2u}$ (σ^*). The $5a_{2u}$ orbital is primarily a Ru–N antibonding orbital, although it has an important metal contribution. The δ^*–π^* separation, 1.18 eV, is large enough to prevent any appreciable population of higher magnetic states at room temperature, which is consistent with the diamagnetism inferred from NMR results. This gap is about 0.2 eV wider than the gap calculated for the triazeno complex, which can be attributed to the stronger π basicity of DFM according to the previously suggested π-basicity model.[8] Since the bridging –CH group is less electronegative than nitrogen, the energy level of ψ_2 of the –NCHN– group is closer in energy to the δ^* orbital of the metal core than is the corresponding ψ_2 orbital of the triazeno ligand, which results in a greater mixing between them and therefore a larger δ^*–π^* separation. A corresponding change in the charge distribution of the δ^* orbital is also observed: the nitrogen contribution is 33% in $Ru_2(DFM)_4$ and 31% in the triazeno complex.

The interesting features shown by the well-resolved UV–vis–near-IR electronic absorption spectrum of $Ru_2(DFM)_4$ (Figure 3) make it tempting to undertake an assignment. Excitation energies for several dipole-allowed transitions (to both singlet and triplet excited states) were calculated by using the transition-state technique, and the results are listed in Table V. The $2b_{1u}$ and $4a_{2u}$ orbitals are the only virtual orbitals considered. The next virtual orbital $6a_{1g}$ is too high to be accessible within the energy range measured. The transitions to both $2b_{1u}$ and $4a_{2u}$ from the

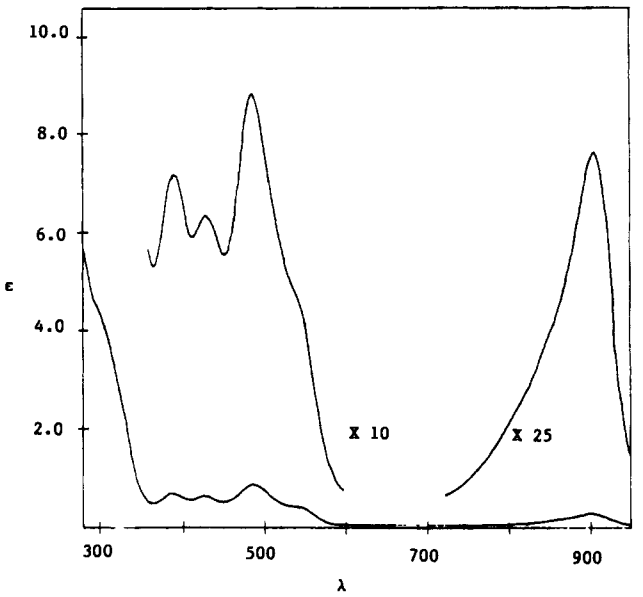

Figure 3. UV–vis spectrum of $Ru_2(DFM)_4$ plotting $\epsilon(10^4\ M^{-1}\ cm^{-1})$ vs λ (nm).

occupied $1a_{1u}$, $6e_u$, $5a_{1g}$, and $5e_u$ orbitals were also skipped in the calculation, since they are all dipole-forbidden.

We find that there is not good quantitative agreement between the calculated singlet–singlet transition energies and the measured peak positions. This is not entirely unexpected for a molecule with such an electron-rich multiple metal–metal bond, since the exchange-correlation interaction of a two-electron process cannot be accurately described by a single Slater determinant SCF calculation. However, by assuming that the order of the transition energies is given correctly by the calculations, and also considering the peak intensities and spin–orbit coupling effect, we tentatively assign the absorption spectra as follows in ascending order of energy: 907 nm, $^3(\pi^* \rightarrow \delta^*)$ and $^3(\pi^* \rightarrow \sigma^*)$; 540 nm (sh), $^3(\delta \rightarrow \delta^*)$; 492 nm, $^1(\pi^* \rightarrow \delta^*)$; 434 nm, $^1(\pi^* \rightarrow \sigma^*)$; 396 nm, $^1(\delta \rightarrow \delta^*)$; 305 nm (sh), $\pi(N) \rightarrow \delta^*$ and σ^*. More detailed reasons for these assignments are as follows.

First, the strong absorption around 305 nm appears to be LMCT because its oscillator strength f ($f \sim \int \epsilon(\nu)\, d\nu$) is overwhelmingly larger than for any other peaks in the visible region. Its broadness (nota bene, the spectrum was recorded in the reciprocal energy scale) indicates a possible overlap of two different charge-transfer transitions. The measured maximum corresponds

to an energy (32800 cm^{-1} or 4.07 eV) much higher than those calculated by Xα, which suggests that there may be a systematic underestimation in the calculation.

With respect to the transition of lowest energy (907 nm or 11030 cm^{-1}), we recall that a similar one in the triazeno complex was initially assigned as a $\pi^* \rightarrow \sigma^*$(Ru-N) transition.[5] From the above discussion of the electronic structures, it is clear that the lowest energy transition should be $\pi^* \rightarrow \delta^*$ (i.e. HOMO → LUMO) transition instead. There are two possible absorptions related to this transition, i.e., $^1A_{1g} \rightarrow {}^1E_u$ and $^1A_{1g} \rightarrow {}^3E_u$, and the latter is spin-forbidden and of lower energy. However, the strong spin-orbit coupling that prevails among the second and third transition series elements can induce substantial intensity for such a normally spin-forbidden transition. In the cases of both $Pt(CN)_4^{2-}$ [24] and $Ir(CN\text{-}t\text{-}Bu)_4^+$,[25] the singlet-triplet ($^1A_{1g} \rightarrow {}^3E_u$) transition of metal-localized $d_\pi(d_{xz,yz}) \rightarrow \pi^*(pz)$ character was observed with an ϵ_{max} as high as one-third that of the corresponding singlet-singlet ($^1A_{1g} \rightarrow {}^1E_u$) transition; the separations between ^1E_u and ^3E_u were determined as 6820 and 8600 cm^{-1} for Pt and Ir complexes, respectively. Considering the possible underestimation previously mentioned and the relative intensities of the peaks, we assign the absorptions at 905 and 492 nm as $^{3,1}(\pi^* \rightarrow \delta^*)$ ($^1A_{1g} \rightarrow {}^{3,1}E_u$), respectively. The ratio $\epsilon_{max}(904)/\epsilon_{max}(492)$ is also about one-third. According to the relative order given by the calculation the weaker peak next to $^1(\pi^* \rightarrow \delta^*)$ at 434 nm can be attributed to the $^1(\pi^* \rightarrow \sigma^*)$ ($^1A_{1g} \rightarrow {}^1E_u$) transition. The intensity of this transition is smaller than that of $^1(\pi^* \rightarrow \delta^*)$ perhaps because there is less ligand mixing in the σ^* orbital. Its singlet-triplet counterpart $^3(\pi^* \rightarrow \sigma^*)$ is not obvious in the spectrum, probably because it is covered by the high-energy tail of the $^3(\pi^* \rightarrow \delta^*)$ transition. It is now not difficult to locate the $^1(\delta \rightarrow \delta^*)$ ($^1A_{1g} \rightarrow {}^1A_{2u}$) transition at 396 nm, in accord with the order from Xα calculation. While the intensity of a purely metal-based $\delta \rightarrow \delta^*$ transition is known to be inherently low,[26,27] this transition is very intense due to the appreciable ligand character in both the δ and δ* orbitals. The $^3(\delta \rightarrow \delta^*)$ ($^1A_{1g} \rightarrow {}^3A_{2u}$) transition is assigned to the shoulder around 540 nm.

From the above assignment the singlet-triplet separation for the metal-based excited configurations can be estimated in the range 7000-9000 cm^{-1}, which is in good agreement with the estimation we suggested in the discussion of the magnetic structure.[2,8]

Acknowledgment. We thank the National Science Foundation for support. Dr. X. Feng is acknowledged for sharing his expertise in SCF-Xα calculations.

Supplementary Material Available: Complete tables of crystal data, bond distances and angles, and anisotropic displacement parameters and a full list of the valence molecular orbitals (8 pages); a table of observed and calculated structure factors (16 pages). Ordering information is given on any current masthead page.

(24) Cowman, C. D.; Gray, H. B. *Inorg. Chem.* **1976**, *15*, 2823.
(25) Smith, D. C.; Miskowski, V. M.; Mason, W. R.; Gray, H. B. *J. Am. Chem. Soc.* **1990**, *112*, 3759.
(26) Cotton, F. A.; Wilkinson, G. *Advanced Inorganic Chemistry*, 5th ed.; John Wiley & Sons: New York, 1988; p 1089.
(27) Hopkins, M. D.; Gray, H. B.; Miskowski, V. M. *Polyhedron* **1987**, *6*, 705.

Contribution from the Departments of Chemistry and Physics, University of Oulu, Linnanmaa, SF-90580 Oulu, Finland, and Department of Chemistry, University of Joensuu, SF-80100 Joensuu, Finland

Chalcogen Ring Interconversion Pathways. ^{77}Se NMR Spectroscopic Study of the Decomposition of 1,2,3,4,5-Se_5S_2 to 1,2,3,4,5,6-Se_6S_2 and 1,2,3,4-Se_4S_2

Pentti Pekonen,[1a] Yrjö Hiltunen,[1b] Risto S. Laitinen,*[,1a] and Tapani A. Pakkanen[1c]

Received January 8, 1991

The decomposition of both natural-abundance and ^{77}Se-enriched 1,2,3,4,5-Se_5S_2 in CS_2 solution has been monitored with ^{77}Se NMR spectroscopy. The freshly prepared samples showed only signals due to 1,2,3,4,5-Se_5S_2. When samples are allowed to stand in the CS_2 solution, additional resonances are observed. Comparison of the natural-abundance spectrum with that from the enriched sample enabled the assignment of these additional resonances to 1,2,3,4-Se_4S_2 and 1,2,3,4,5,6-Se_6S_2 to be made. The simulation of the enriched spectrum yielded the ^{77}Se-^{77}Se coupling constants. All transitions could be assigned with an excellent fit. The NMR results show that the decomposition of 1,2,3,4,5-Se_5S_2 proceeds with a selenium atom transfer from one seven-membered ring molecule to another.

Introduction

Compounds containing cumulated S-S bonds are known to undergo interconversion reactions. Typical examples are the decomposition of thermodynamically unstable sulfur molecules with the formation of stable S_8,[2] the decomposition of S_8 in the molten state or in organic solvents,[3] the polymerization and depolymerization of liquid sulfur,[2] the decomposition of organic polysulfanes R_2S_n on heating,[4] and the vulcanization of rubber.[5] Similar interconversion reactions have also been observed for selenium. When Se_8 is dissolved in CS_2, an equilibrium between Se_6, Se_7, and Se_8 is rapidly set up.[6] Analogous decomposition of S_8 is much slower in CS_2 and requires heating.[7] In acetonitrile, however, the equilibrium is instantaneously established.[8]

The mechanism of such interconversion reactions is not known. Though several alternative pathways have been suggested (for a review, see ref 9), the lack of rigorous experimental evidence

(1) (a) Department of Chemistry, University of Oulu. (b) Department of Physics, University of Oulu. (c) University of Joensuu.
(2) Steudel, R.; Passlack-Stephan, S.; Holdt, G. *Z. Anorg. Allg. Chem.* **1984**, *517*, 7.
(3) (a) Steudel, R.; Strauss, R.; Koch, L. *Angew. Chem.* **1985**, *97*, 58; *Angew. Chem., Int. Ed. Engl.* **1985**, *24*, 59. (b) Steudel, R.; Strauss, R. *Z. Naturforsch.* **1982**, *37B*, 1219.
(4) (a) Kende, I.; Pickering, T. L.; Tobolsky, A. V. *J. Am. Chem. Soc.* **1965**, *87*, 5582. (b) Pickering, T. L.; Sauders, K. J.; Tobolsky, A. V. *J. Am. Chem. Soc.* **1967**, *89*, 2364.
(5) Porter, M. In *Perspectives in the Organic Chemistry of Sulfur*; Zwanenburg, B., Klunder, A. J. H., Eds.; Elsevier Science Publishers: Amsterdam, 1987; p 267.
(6) (a) Steudel, R.; Strauss, E.-M. *Z. Naturforsch.* **1981**, *36B*, 1085. (b) Laitinen, R. S.; Pakkanen, T. A. *J. Chem. Soc., Chem. Commun.* **1986**, 1381.
(7) Steudel, R. In *Sulfur—its Significance for Chemistry, for the Geo-, Bio-, and Cosmosphere and Technology*; Müller, A., Krebs, B., Eds.; Elsevier Science Publishers: Amsterdam, 1984; p 3.
(8) Tebbe, F. N.; Wasserman, E.; Peet, W. G.; Vatvars, A.; Hayman, A. C. *J. Am. Chem. Soc.* **1982**, *104*, 4971.

0020-1669/91/1330-3679$02.50/0